X-641-73-88

PREPRINT

EXPECTED GAMMA-RAY EMISSION SPECTRA FROM THE LUNAR SURFACE AS A FUNCTION OF CHEMICAL COMPOSITION

FEBRUARY 1973

GSFC

GODDARD SPACE FLIGHT CENTER

GREENBELT, MARYLAND

X-641-73-88

EXPECTED GAMMA-RAY EMISSION SPECTRA FROM THE LUNAR SURFACE AS A FUNCTION OF CHEMICAL COMPOSITION

R. C. Reedy,* J. R. Arnold

Department of Chemistry

University of California, San Diego

La Jolla, California 92037

and

J. I. Trombka

Goddard Space Flight Center

Greenbelt, Maryland 20771

February 1973

*Now at Los Alamos Scientific Laboratory
Los Alamos, New Mexico 87544

GODDARD SPACE FLIGHT CENTER

Greenbelt, Maryland

EXPECTED GAMMA-RAY EMISSION SPECTRA FROM THE LUNAR SURFACE AS A FUNCTION OF CHEMICAL COMPOSITION

R. C. Reedy,* J. R. Arnold

Department of Chemistry

University of California, San Diego

La Jolla, California 92037

and

J. I. Trombka

Goddard Space Flight Center

Greenbelt, Maryland 20771

ABSTRACT

The gamma-rays emitted from the moon or any similar body carry information on the chemical composition of the surface layer. The elements most easily measured are K, U, Th and major elements such as O, Si, Mg and Fe. The expected fluxes of gamma-ray lines are calculated for four lunar compositions and one chondritic chemistry from a consideration of the important emission mechanisms: natural radioactivity, inelastic scatter, neutron capture, and induced radioactivity. The models used for cosmic-ray interactions are those of Reedy and Arnold (1972) and Lingenfelter et al (1972). The areal resolution of the

*Now at: Los Alamos Scientific Laboratory
Los Alamos, New Mexico 87544

experiment is calculated to be around 70-140 km under the conditions of the Apollo 15-16 experiments. Finally, a method is described for recovering the chemical information from the observed scintillation spectra obtained in these experiments.

INTRODUCTION

A planetary body whose atmospheric thickness is not too large emits gamma-ray lines whose intensity can be observed by orbital remote sensing and used to determine the mean concentration of a number of elements in the upper tens of centimeters of the surface being observed. Experiments to gain knowledge about the chemical composition of the Moon, Mars, Mercury, and other bodies in this way have been proposed many times. Up to the present only the Moon has actually been studied. Metzger et al (1964) placed an experiment on Rangers 3, 4, and 5. None of these was able to make measurements near the moon, but the deep space flux was successfully recorded. Vinogradov et al (1967) placed a small detector on Luna 10, which orbited the moon. Successful experiments were carried out on Apollo 15 and 16 (Metzger et al, 1973).

In the present paper we calculate the expected spectrum of gamma-ray line emission from the moon, as observed from a detector above the lunar surface, for a range of known and possible chemical compositions, primarily with reference to the Apollo missions.

The experimental technique, and the present theoretical treatment, are equally applicable to any atmosphereless planetary body such as Mercury, an asteroid, or a planetary satellite. For the special case of Mars, whose atmospheric depth is of the order of the photon interaction length, significant corrections for absorption are required, but the experiment is still quite practical

(Metzger and Arnold, 1970; Surkov et al, 1971). The modifications in the theory required for planetary bodies other than the moon are not great, and will be noted below where appropriate.

Gorenstein and Gursky (1970) have made a calculation of gamma-ray line emission from the moon, and have reviewed the previous literature. Armstrong (1972) has used a Monte Carlo method to derive the flux of the stronger lines and of the continuum from the moon. The present work is based on a more detailed theoretical model developed mainly for lunar sample studies by Reedy and Arnold (1972). The reader interested in a more complete discussion of this and other models of cosmic-ray interaction with the lunar surface should consult that paper.

In this paper we calculate the fluxes for a number of gamma-ray lines produced by the major sources of line radiation in the moon: decay of naturally occurring primordial radioactive nuclei (K, U, and Th), prompt processes (inelastic scattering and neutron capture) involving secondary neutrons produced by galactic-cosmic-ray bombardment, and decay of radionuclides produced by galactic-cosmic-ray and solar-cosmic-ray bombardments. The fluxes from a semi-infinite plane are calculated for five representative chemical compositions: Apollo 11, Apollo 12, Apollo 14, lunar anorthosite, and chondrite. The spatial resolutions and fluxes relative to an isotropic detector in orbit about the moon are determined for the major sources of gamma-rays.

We emphasize the line spectrum because it contains the chemical information. However, it is now clear that the continuum emitted from the lunar surface has a substantially larger flux than the sum of all lines in the energy region of interest (Metzger et al, 1973). Thus it must be accurately determined in order to derive correct line intensities.

Once the production mechanisms are understood, and the relation between line intensity and chemical abundance defined as well as possible by theory, there remains the problem of deriving the actual photon flux from the observed pulse height spectrum in the detector. We give a systematic account of the methods used to obtain these fluxes (including the determination of the continuum, treated here as an unknown) and hence derive chemical composition, from the experimental data.

Sources of Line Radiation. The most direct observations of chemical composition which are possible by this technique are those of the elements K, Th, and U. These elements and their radioactive daughters emit gamma-rays as given in Table 1. These "natural" gamma-rays are emitted at a steady and predictable rate. Except for disequilibrium caused by radon emanation which at the present writing seems to be relatively unimportant for gamma emission processes (Gorenstein and Bjorkholm, 1972), the calculation of emission rates is quite simple.

The other important sources of line radiation all originate in the bombardment by high energy particles (cosmic-rays). Because of the high energy of the cosmic-rays, every possible mechanism of nuclear excitation is active. In particular, the positron annihilation line at 0.511 MeV is excited by a wide variety of mechanisms. For this reason little chemical information can be derived from its intensity. In other cases only a small number of elements can produce a given line.

High energy particles from outside the solar system, the so-called galactic-cosmic-rays (GCR), bombard the lunar surface continuously, with intensity varying slowly over the solar cycle. The interactions of this primary flux with a solid body give rise to numerous secondary particles. Those of greatest importance to gamma-ray production are the particles in the energy range 1-100 MeV, which consist almost entirely of neutrons. The spectra of the primary and secondary particles are discussed in detail by Reedy and Arnold (1972).

Of the many possible mechanisms for emission of nuclear gamma-ray lines, only three are important for our purposes. These are neutron inelastic scattering, neutron capture, and induced radioactivity. Neutrons with energies above the first excited state of a nucleus can inelastically scatter, exciting states which promptly de-excite by gamma-ray emission. There are also several cases of prompt gamma-rays from other neutron-induced (n,xγ) reactions. Low energy

neutrons can be captured by nuclei and produce gamma-rays via (n, γ) reactions. Nuclear reactions can also produce radioactive species, some of which emit gamma-ray lines in high yields.

The sun also emits energetic particles, the so-called solar-cosmic-rays (SCR). These are also chiefly protons, usually having energies of less than 100 MeV. The flux is intermittent, a given storm lasting only a few days. These storms are concentrated in the years around solar maximum. Only the gamma-rays resulting from the decay of induced-radioactive nuclei are calculated here.

Chemistry. The gamma-ray experiment is capable of measuring the composition of a lunar or planetary surface over a very wide range. To be realistic we have chosen in this paper to present calculations for five chemical compositions. The analyses performed at the Surveyor V site (Turkevich et al, 1969) are so similar to the more detailed data on the Apollo 11 soil that it is reasonable to accept the latter as representative of Mare Tranquillitatis, over which the Apollo 15 Command Service Module flew. Thus the Apollo 11 results represent probable "ground truth". The Apollo 12 soil gives the best information we have on the composition of the area of Oceanus Procellarum. The chemical compositions used for the Apollo 11 and 12 lunar soils are the average values compiled by J. Warner, MSC, as given by Schnetzler and Nava (1971). The Apollo 14 soil (Schnetzer and Nava, 1971) from the Fra Mauro region, corresponds closely to what Hubbard

and Gast (1971) have called KREEP. They suggest that this type of material may be widespread on the lunar surface. The "lunar anorthosite" component has been suggested by Wood et al. (1970) as a major constituent of the highlands.

Finally, we have used an ordinary chondritic composition (Mason, 1962) very different from anything yet encountered or expected as a main component on the moon. We consider it as a possible asteroidal or planetary surface composition. The chemical compositions are given in Table 2.

Calculation of the Total Emitted Flux. Before discussing the expected gamma-ray source strengths as a function of depth, we will give the method of calculating the flux emitted for a given source strength. We are not here concerned with scattered photons, which contribute only to the continuum, but only those which undergo no interactions before reaching the surface. There are two different quantities that can be used to represent the intensity of photons leaving the lunar surface—the flux, the intensity of photons reaching a unit-area isotropic detector above the lunar surface, and the current or albedo, the intensity of photons passing through a unit-area of (or parallel to) the lunar surface. Only the flux will be discussed and calculated below.

In the expressions below, the depth below the surface, x will be in units of g/cm^2 and the gamma-ray source strength at depth x is A(x) in units of disintegrations per unit mass and time. The calculations will be for a monoenergetic photon which passes through lunar material with an exponential

mass attenuation coefficient μ (in units of cm^2/g). All calculations will be for a semi-infinite plane source.

The flux of photons at an isotropic detector above a semi-infinite plane resulting from photons emitted at a depth x below the surface is

$$I(x) = \int_0^{2\pi} d\phi \int_0^{\frac{\pi}{2}} \sin\theta \, d\theta \, \frac{A(x)}{4\pi} \sec\theta \, e^{-\mu x \sec\theta}, \tag{1}$$

where $A(x)/4\pi$ is the rate of photon emission per unit solid angle at depth x, θ is the angle with respect to the normal, and $e^{-\mu x \sec\theta}$ is the fraction of the photons emitted from a depth x and with angle θ that escape from the surface. The sec θ term is the area of the moon's surface that a unit area of detector projects for an angle θ with respect to the normal. Equation (1) integrates over solid angles to give the contribution of the flux at the detector from a source at depth x in the moon

$$I(x) = \frac{A(x)}{2} \epsilon_0(\mu x). \tag{2}$$

ϵ_0 (μx) is a Gold integral (Rossi, 1952) and is the same as -Ei(-μx), where Ei is the exponential integral. For a source whose activity is constant with depth, Equation (2) can be integrated over depth to yield the total flux at the detector,

$$I = \frac{A}{2\mu}. \tag{3}$$

The expression for the current from a depth x is the same as Equation (1), but without the sec θ term and, when integrated over all angles and depths for a

constant source, gives as the current $A/4\mu$, which is half the corresponding value for the flux (Equation (3)).

In the calculations for all sources but natural radioactivity, Equation (2) was used to derive the flux at each depth and the integration over depth was done numerically. A series (about 50) of planar layers were used, with many layers near the surface and fewer layers at greater depths. A(x) is calculated for each source for the depth x in the middle of each layer and I(x) determined for that layer. I(x) is then multiplied by the thickness of the layer and these products for all layers are summed to get the total flux from the semi-infinite plane. Using a constant source in this numerical integration results in a value for the flux within one percent of the exact value from Equation (3).

The values used for the mass attenuation coefficient μ were those for aluminum (White, 1952), which is a very close parallel to that for natural silicate rocks. In the region of interest from 0.5 to 10 MeV μ decreases from about 0.083 cm^2/g (mean thickness of 12 g/cm^2) to 0.023 cm^2/g (mean thickness of about 44 g/cm^2). For a source uniform with depth, half the flux at the detector comes from depths of less than 0.27 of the mean thickness ($1/\mu$) and 90% from depths of less than 1.3 mean thicknesses.

CALCULATED FLUXES

To a first approximation the expected flux of a line due to a particular element might be expected to be proportional to its concentration. There are

effects, however, which can cause a departure from a simple proportionality to abundance. Some of these are small in realistic cases. Thus the range of density and mean atomic number is small enough in probable examples that the development of the nuclear cascade, and the mass absorption coefficients of the emitted gamma-rays, are not significantly affected. However, an iron-nickel object, or one made up of "ices," would require a new analysis. The most important non-linear phenomena threated here involve the thermalization and capture of neutrons and are discussed below.

Natural Radioactivity. The naturally occurring primordial radioactive nuclei—uranium, thorium, and their daughters, and K^{40}—were assumed to be uniformly disturbed to a depth of several meters at the lunar surface. All daughter isotopes were assumed to be in equilibrium with their parent, and the radon daughters of uranium and thorium were assumed not to have diffused from the location at which they were formed. For the emission of photons from a uniform source, the flux at an isotropic detector above a semi-infinite plane was calculated using Equation (3). The value used for the source strength A in Equation (3) for a specific gamma-ray was the disintegration rate of the parent nucleus multiplied by the yield of the gamma-ray per disintegration. The important parameters and the calculated line intensities for the gamma-rays resulting from the decay of naturally occurring radioactive nuclei are given in Table 1. The calculated fluxes agree quite well with those of Armstrong (1972),

and, after dividing by the factor of 2, with the currents calculated by Gorenstein and Gursky (1970). The gamma-ray intensities for the decay of V^{50}, Lu^{176}, and La^{138} were found to be negligible.

Solar-cosmic-ray Induced Radioactivity. The solar-cosmic-rays are emitted irregularly from the sun in a few intense solar flares around the period of solar maximum during the 11-year solar cycle. Only those gamma-rays that result from the decay of radionuclides produced by solar protons need be considered, since high intensity of charged particles during a solar flare would essentially saturate the actual detector system and make the detection of prompt solar-cosmic-ray produced gamma-rays (or other gamma-rays) virtually impossible. Since the solar-cosmic-rays consist mainly of low energy protons with relatively few particles having energies above 100 MeV, the major induced activities in the moon are produced by (p,n), (p,pn), and similar low energy nuclear reactions. The dominant gamma-ray emitting isotopes produced by solar protons in the moon are Co^{56}, Mn^{54}, V^{48}, Na^{22}, and Al^{26}.

The production rates for solar-cosmic-ray induced radionuclides as a function of depth in the moon which were used in this work are those calculated by Reedy and Arnold (1972). These calculations were made assuming a rigidity spectral shape for the incident solar proton flux

$$\frac{dJ}{dR} = k \exp(-R/R_0) \qquad (4)$$

where R is the rigidity of the proton (R = pc/ze, p = momentum) in units of megavolts (MV) and R_0 is the parameter that determines the shape of the flux spectrum. Finkel et al (1971) found that production rates calculated using rigidity spectral shapes agreed very well with the observed activities of solar-cosmic-rays produced radionuclides in rock 12002. Details of the calculation of the production rates versus depth for solar-cosmic-ray induced radionuclides are given in Reedy and Arnold (1972). For all SCR-produced radionuclides, the production rates decrease rapidly with depth.

Table 3 gives the calculated photon leakage intensities for the major solar-cosmic-ray induced radionuclides. Since the actual activity of each isotope depends on the intensity and spectral shape of the solar-cosmic-rays during the last few half-lives of the isotope (Reedy and Arnold, 1972), the results given here are for three different spectral shapes—values of R_0 of 50, 100, and 150 MV—and for a steady state solar proton flux with the normalization that the integral omnidirectional flux of particles in space with energies above 10 MeV was 100 protons/cm^2sec. These values are consistent with the solar-induced activities observed by Finkel et al (1971) and Wahlen et al (1972), which corresponded to values of R_0 in the range of 80 to 100 MV and with equivalent steady state fluxes having integral normalizations above 10 MeV ranging from 75 to 160 protons/cm^2sec. The calculated intensities of Table 3 for Mn^{54}, Na^{22}, and Al^{26} are about the same as the corresponding intensities resulting from the production of these nuclides from galactic-cosmic-rays (Table 4). Since their

half-lives are relatively long, yet shorter than the 11-year solar cycle, Mn^{54} and Na^{22} have slowly varying solar-cosmic-ray induced activities during a solar cycle. The long-lived Al^{26} has no variation in activity during a solar cycle. The very short-lived isotopes Co^{56} (77-day) and V^{48} (16-day) are made in only trace amounts by galactic-cosmic-rays and their activities will vary considerably during a solar cycle, depending on the solar flares during their last few mean lives. The agreement of the fluxes calculated here with those calculated by Armstrong (1972) is poor, due in part to the fact that he did not consider protons with energies of less than 30 MeV.

For bodies further from the sun the SCR contribution will be even smaller, but the rate of decrease is not well known.

Galactic-Cosmic-Rays. The galactic-cosmic-rays are high energy particles that continuously bombard the moon, producing many secondary particles as a result of the nuclear cascades they produce. The most important particle for inducing nuclear reactions in the moon is the neutron, approximately 10 neutrons being produced per incident galactic-cosmic-ray particle. These neutrons travel through the moon until they are removed by nuclear interactions or until they escape from the lunar surface. Secondary charged-particles are less important since most of them have relatively low energies and usually are stopped by ionization-energy-losses before they have a chance to undergo nuclear interactions.

Neutrons with energies of about 1 MeV and greater can produce gamma-rays by exciting levels of nuclei by inelastic scattering reactions of the $(n,x\gamma)$ type, where x is usually a neutron but can be other particles. Galactic-cosmic-rays can also produce gamma-ray emitting radionuclides in spallation reactions. The production rates for both of these types of reactions were calculated using the galactic model of Reedy and Arnold (1972). Neutrons with energies below the first excited level of the nuclei in the moon can be elastically scattered by nuclei, escape from the moon, or be captured by nuclei through the (n,γ) reaction. In the process of neutron capture, prompt gamma-rays are emitted during the de-excitation of the product nucleus, which, in (n,γ) reactions is formed in excited levels that are about 8 MeV above their ground states. Some nuclei formed as a result of neutron capture are radioactive and emit gamma-rays in their decay. For the neutron capture reactions, the lunar neutron-capture rates of Lingenfelter et al (1961) and Lingenfelter et al (1972) were used, as described below.

The rates for inelastic scattering reactions and for the production of radionuclides at a depth x were calculated by integrating over all energies the product of the differential flux of galactic particles at that depth and the excitation function for the reaction

$$A(x) = N \int_0^\infty dE \frac{dJ}{dE}(E,x)\, \sigma(E) \qquad (5)$$

with N being the number of target nuclei. The differential fluxes of galactic particles as a function of depth in the moon were taken from Reedy and Arnold (1972). For $(n,x\gamma)$ reactions, A(x) increases with depth until a depth of about 50 g/cm^2. Below that depth A(x) decreases with depth. For the production of radionuclides, the increase with depth is less, the reactions with the higher energy thresholds having less increase.

Since the differential flux of galactic secondary particles decreases rapidly with energy (Reedy and Arnold, 1972), most of the intense gamma-ray lines result from reactions which have large cross-sections at low energies. Almost all of the $(n,x\gamma)$ reactions producing important gamma-ray lines have their largest cross-sections at relatively low energies, usually at energies below 20 MeV and often as low as 1 MeV or less for some of the $(n,n\gamma)$ reactions. The reactions that produce the largest yields of radioactive nuclei are low-energy reactions such as the (n,p), (n,α), and (n,2n) reactions. In some cases, these radioactive nuclei decay through the same levels of their residual nuclei as are excited by $(n,n\gamma)$ inelastic scattering reactions on these nuclei. Thus the $Al^{27}(n,\alpha)Na^{24}$ and the $Mg^{24}(n,p)Na^{24}$ reactions result in the same lines at 1.369 and 2.754 MeV as are produced by $Mg^{24}(n,n\gamma)Mg^{24}$ reactions. Most of the excitation functions used in these calculations were based on experimental cross-sections. The references are cited in Table 4.

The calculated gamma-ray line intensities for the most intense lines for O, Mg, Al, Si, Ca, Ti, and Fe are given in Table 4 by element in order of decreasing intensity. The intensities for gamma-ray lines resulting from neutron capture reactions are given and discussed separately below. Generally, the most intense line for each element for reactions other than neutron capture is that resulting from $(n, n\gamma)$ reactions exciting the first excited level of the most abundant isotope. Usually it is at an energy of less than 2 MeV. Several elements have their first excited levels at higher energies, such as Ca^{40} and O^{16} at 3.73 and 6.129 MeV, respectively. Several elements have strong gamma-ray lines resulting from prompt reactions other than the $(n, n\gamma)$ reaction, such as the $O^{16}(n, a\gamma)\ C^{13}$ lines between 3 and 4 MeV.

The rates for the capture of low energy (thermal and epithermal) neutrons in the moon have been calculated for several chemical compositions by Lingenfelter et al (1961) and Lingenfelter et al (1972). Assuming a source spectrum of neutrons with energies below 10 MeV, the authors solved a multigroup transport equation to get the equilibrium energy spectrum and spatial distribution of the lunar neutron flux. They found that the calculated neutron flux was strongly dependent on the assumed composition of the lunar surface, the important compositional variables being the macroscopic capture cross-sections for the major elements, hydrogen content of the lunar surface, and the concentration of the rare earth elements Gd and Sm.

The presence of significant amounts of hydrogen in any region of the lunar surface would decrease the neutron leakage flux, increase the ratio of capture at low neutron energies to that at higher energies, and increase the capture rate in the top 150 g/cm^2 of the lunar surface (Lingenfelter et al, 1961). The total macroscopic capture cross-section (for nuclei with 1/v capture cross-sections) affects the energy spectrum since it changes the probability of being captured before reaching thermal energies if this cross section is larger. The rare earth el ments Gd and Sm have very large capture cross-sections near thermal energies and can capture a significant fraction of the thermal neutrons.

The total neutron capture rates of Lingenfelter et al (1972) and R. E. Lingenfelter and E. H. Canfield (private communication, 1971) were used in the calculation of the intensities of gamma-ray lines resulting from neutron capture. The rate for neutron capture increases significantly with depth to a depth of about 150 g/cm^2, below which the rate decreases with depth. The ratio of the neutrons captured to the neutrons escaping from the moon was not very sensitive to the total macroscopic neutron capture cross-section. The total macroscopic neutron capture cross-sections for the Apollo 12 lunar fines, the Apollo 14 lunar fines, and the lunar anorthosite are 0.78, 0.68 and 0.37, respectively, for that for the Apollo 11 lunar fines, but their total neutron capture rates were 0.97, 0.95, and 0.83, of the rate for the Apollo 11 fines. The main factor in determining the rate of neutron capture by a specific element is the fraction of the total macroscopic neutron capture cross-section that the element contributes for that

chemical composition. The ratio of the fraction of the neutrons captured by an element to the weight fraction of that element is inversely proportional to the total macroscopic capture cross-section for a given chemical composition. For example, in the Apollo 11 lunar fines, iron (12.3% by weight) captures 35% of the neutrons, but in a lunar anorthosite (2.7% iron by weight), it captures 21% of the neutrons, whereas silicon (about 21% by weight in both) captures 8% and 22% of the neutrons in these two chemical compositions, respectively. All elements except the rare earth elements were assumed to capture neutrons with 1/v cross-sections. The contribution of the rare earth elements Gd and Sm were estimated using the equivalent 1/v cross-sections calculated by Lingenfelter et al (1972) for these elements. (For the Apollo 11 lunar fines, the effective cross-section for Gd is 18% of its thermal cross-section and Gd captures 6% of all the neutrons.) The 1/v cross-sections used for the major elements were measured at 0.023 eV (2200 m/sec) and were taken from Bartholomew et al (1967), except for the value of 0.176 barns which was used for Si (Maddison and Jones, 1969).

The yields per neutron capture for the prompt gamma-rays were taken from Bartholomew et al (1967). The neutron-capture gamma-ray energies and yields for neutrons captured above thermal energies were assumed to be the same as those for thermal neutrons, even though a major portion of the lunar neutrons are captured before they reach thermal energies. The yields per disintegration

for gamma-rays resulting from the decay of radioactive product nuclei were those of Lederer et al.(1967). The photon fluxes for the major lines of each element were calculated by numerically integrating Equation (2) and are given in Table 5 for the Apollo 11 chemical composition.

The ratio of the gamma-ray flux for a given line to the weight fraction of the element varies with chemical composition. For the Apollo 12, Apollo 14, lunar anorthosite, and chondritic chemical compositions, this ratio of flux to weight fraction is 1.25, 1.40, 2.27, and 1.46 times that of the Apollo 11 composition.

The only difference among the chemical compositions affecting the neutron capture rates for all of these compositions but the chondritic composition was the total macroscopic cross-section and the fraction of the total captures each element contributed. The major difference between the Apollo 11 lunar fines and the chondritic composition was that the chondritic composition was arbitrarily assumed to include 0.1 atoms of hydrogen for each atom of silicon. This addition of hydrogen raised the ratio of the photon flux to the weight fraction for each element by a factor of about 1.4. A hydrogen to silicon atomic ratio of 1 would raise this ratio by a factor of about 2.7 above the ratio for no hydrogen.

Gamma-ray lines for the rare earth elements Gd and Sm are not given here since they have few neutron capture lines with yields per capture greater than

a few percent. The main effect of these rare earth elements is to decrease the intensities of the major lines for all other elements. If there were no rare earth elements in the Apollo 11, 12, and 14 lunar fines, the intensities of the lines for all other elements would be raised by factors of 1.06, 1.11, and 1.25, respectively. Only for the Apollo 14 chemistry, where the elements with high thermal capture cross-sections, iron and titanium, are low and where the rare earth elements are very abundant, does the capture of neutrons by rare earth elements significantly affect other gamma-ray line intensities.

The calculated production rates for $(n, x\gamma)$ and (n, γ) reactions are for the average GCR flux near the earth during a solar cycle. Since the GCR flux is somewhat lower at solar maximum and higher at solar minimum than the average flux used here (Webber, 1967), the actual production rates will vary with the solar cycle. Thus the gamma-ray flux for all sources except those from the decay of long-lived isotopes will vary during the solar cycle. Since all GCR produced lines will have approximately the same variations, only the average flux for the gamma-ray lines are given here. A modest scale correction determined from cosmic-ray data must be applied for the time of each mission. The gamma-ray fluxes expected from other large bodies in the solar system should be similar to those calculated here, as the intensity of the high energy GCR particles does not vary significantly with distance from the sun.

The fluxes calculated for the prompt GCR produced lines agree fairly well with those calculated by Armstrong (1972) using a Monte Carlo method. The currents for the neutron capture lines agree well with the calculated currents of Gorenstein and Gursky (1970), while their results for the lines resulting from $(n, x\gamma)$ reactions are about twice our values. The disagreement for the $(n, x\gamma)$ reactions is probably due to the fact that they used a simpler model for these reactions than the one used here.

Calculated Fluxes. The fluxes from a semi-infinite plane of the major gamma-ray lines for each of the five chemical compositions of Table 2 are shown in Figures 1 and 2. The fluxes include the contributions from the decay of the natural radioactive nuclides, from all the galactic-cosmic-ray sources, including both prompt-$(n, x\gamma)$ and (n, γ)—and decay photons, and from the decay of solar-cosmic-ray produced nuclides for an incident solar proton spectral shape $R_0 = 100$ MV and a 4π proton integral flux above 10 MeV of 100 protons/ $cm^2 sec$. The line at 511 keV resulting from the annihilation of positrons was not calculated, because of the many different sources for this line. It is simply indicated in the figures. In addition to the lines shown in Figures 1 and 2, there will be a strong continuum that includes a multitude of minor lines, photons resulting from Compton scattering and bremsstrahlung in the moon. The approximate nature of this continuum is discussed below.

The major lines shown in Figures 1 and 2 are also given in Tables 1, 3, 4, and 5 for the Apollo 11 chemical composition. There are only a few gamma-ray

lines that stand out above the rest. Most of the major lines have about the same magnitudes and there are a large number of such lines, especially below 4 MeV. The major elements whose abundances in the moon are expected to be similar for all likely chemical compositions—oxygen and silicon—have many intense lines. Several elements, such as magnesium, aluminum, and calcium, have most of their most intense lines near other major lines. For example, the $Mg^{24}(n, n\gamma)$ line at 1.369 MeV is at an energy where there are many other lines from such sources as U, Na^{24}, and $Ti(n, \gamma)$. The $Ca(n, n\gamma)$ lines at 3.73 and 3.90 MeV are near the $O^{16}(n, \alpha\gamma)$ lines at 3.68 and 3.85 MeV.

The calculations indicate that there are good gamma-ray lines with which to determine the concentrations in the moon's surface of oxygen, iron, and titanium. Concentrations of thorium, potassium, and uranium can also be readily observed. Calcium, silicon, magnesium and aluminum also have some good gamma-ray lines, although few of their lines are well isolated from other major lines, and, while absolute concentration will be hard to determine, large variations of these elements in the moon should be observable. The other elements do not have very useful gamma-ray lines for expected range of compositions.

SPATIAL RESOLUTION

To understand the possible spatial resolution of the lunar experiment, it is necessary to consider the angular dependence of the system response. Figure 3

shows the basic geometry. For a given detector-source distance ℓ the photons striking the detector are emitted at a fixed angle β from the normal at the source, and strike the detector at an angle θ with respect to the line connecting the detector and the center of the moon. The limiting distance, ℓ_{max}, is the horizon distance, equal to $(2Rh + h^2)^{1/2}$. For a height of 100 km above the moon's surface, ℓ_{max} is 598 km.

For a point source (really a columnar source), or "hot spot", the intensity I' at the detector per unit source area is

$$I' = \frac{a \cos\beta}{4\pi \ell^2} \tag{6}$$

where

$$a = \int_0^\infty A(\cos\beta\ x)\, e^{-\mu x}\, dx \tag{7}$$

For a uniform source, a is A/μ.

By integrating over radius the product of Equation (6) and the moon's surface area at each radius, one can calculate the flux at the detector originating within a circle of radius ρ on the moon's surface. The values for a, β, and ℓ in Equation (6) all vary with ρ. It is of interest also to consider the behavior in crossing a great circle boundary between two extended source regions of different composition, at right angles to the boundary. The flux for beyond the boundary is calculated the same as for the flux for inside a circle, with the integration over radius including an additional factor for the fraction of the circle at radius ρ beyond the boundary.

These calculations were done for four cases: an (n,γ) reaction (the 4.936 MeV line from $Si(n,\gamma)$), an $(n,x\gamma)$ reaction (the 1.369 MeV line from $Mg(n,n\gamma)$), a source uniform with depth (any natural radioactive decay line), and a solar-cosmic-ray produced radionuclide (the 1.809 MeV line of Al^{26} produced by protons on Si). The difference among these cases is the behavior of A(x) in the first few photon mean free paths of the surface: A(x) increases considerably with the depth near the surface for the (n,γ) reaction, increases somewhat with depth for the $(n, x\gamma)$ reaction, and decreases rapidly with depth for the solar-cosmic-ray (SCR) case. The relative fractions of the flux at an isotropic detector 100 km above the lunar surface are given in Figure 3 for point sources, inside a circle, and beyond a boundary, for each of these four cases.

For the uniform source and a detector altitude of 100 km, the distance ρ where I' falls to half the value of the point source for directly below the detector is 73 km. Half the flux at the detector originates inside a circle of radius 118 km. At 68 km from a great circle boundary 75% of the field of view is occupied by the region below the detector and 25% by the region beyond the boundary. Corresponding distances for the SCR case are considerably greater than these. For the $(n,x\gamma)$ and (n,γ) cases, these distances are about 90% and 80%, respectively, of those of the uniform case. GCR-produced radionuclides vary between the uniform case and the $(n,x\gamma)$ case, depending on the excitation function for the reaction.

The SCR-produced radionuclides, where A(x) decreases with depth, are examples of limb brightening, where more photons arrive per unit solid angle at the detector from regions near the limb. The (n,γ) and $(n,x\gamma)$ cases, where A(x) increases with depth near the surface, are examples of limb darkening. Since the flux of photons per unit solid angle at the detector varies with angle for non-uniform sources, the flux at the detector above the moon is not just the flux for a semi-infinite plane times the ratio of the solid angle for the lunar case to that for the semi-infinite plane. For an altitude of 100 km above the moon, this ratio of solid angles is 0.67465, θ_{max} being 71.013°. For this lunar altitude, the ratio of fluxes from the moon to that from a semi-infinite plane is greater than the corresponding ratio for solid angles by a factor of about 1.12 for most (n,γ) cases, 1.07 for most $(n,x\gamma)$ cases, and less by factors of about 0.7 to 0.8 for various SCR cases. For sources uniform with depth, the ratio of fluxes is exactly the same as the ratio of solid angles for all geometries.

DATA REDUCTION

As discussed above the lunar gamma-ray emission spectrum can be considered to be made up of two components: the line spectrum and a spectrum continuous in energy. This continuum can be associated with such processes as Compton scattering of gamma-rays, and bremsstrahlung in the lunar surface. There are also a number of other contributions to the background continuum, such as induced and natural radioactivity in the spacecraft, diffuse sky background, and spallation effects in the detector crystal. From laboratory

experiences and from the analysis of earlier space flight gamma-ray data we find that the total background continuum can be approximated quite closely by a power law distribution in energy. In this section we will describe the analytic method for obtaining the elemental composition from the observed lunar surface spectrum.

We first consider the basic method of inferring photon spectra from an analysis of the measured pulse height spectrum. The pulse height spectrum is a measure of the interaction between the incident gamma-ray and the detector. We can describe this interaction process as follows:

$$Y(V) = \int_0^{E_{max}} T(E)\, S(E,V)dE \qquad (8)$$

where T(E) is the differential energy photon spectrum as a function of energy E, S(E, V) is the detector response function which reflects the mechanisms of converting photons of energy, E, into a pulse height signal, V, at the output of the detector, and Y(V) is the measured "pulse height" spectrum as a function of pulse height V.

The problem is to infer T(E) from Y(V) and a knowledge of the function S(E, V). We now consider the shape of S(E, V) and its variation with energy.

S(E, V) can be either experimentally determined or theoretically calculated, (Bell, 1955; Seltzer and Berger, 1971). Radioactive sources were available

to study this energy dependence in the Apollo detector system (a 2-3/4 x 2-3/4 inch NaI(Tℓ) crystal) experimentally up to 3 MeV. Neutron capture spectra were used to study crystal response up to 10 MeV (Trombka et al, 1971). The energy response functions were also calculated using Monte Carlo techniques and found to be in good agreement with experiment (Trombka et al, 1971; Seltzer and Berger, 1971). We conclude that the response function can be calculated theoretically for any energy needed in the analysis considered in the following discussion. The three pulse height spectra shown in Figure 4 have been produced by the Monte Carlo calculation technique.

The analysis of gamma-ray pulse height spectra in this spectral region must be accomplished by numerical methods because we cannot yet perform the inverse transform analytically. The method for obtaining the best estimate for T(E) is based on a theorem in sampling theory; and on the fact that there is a finite energy resolution of the detection system. The Shannon Sampling Theorem asserts that, if a distribution has no oscillatory component with a frequency greater than f_{max}, then samples at discrete points not farther apart than $1/2\ f_{max}$ describe the original function exactly. The original function may then be reconstructed from the samples (Trombka et al, 1970). The approximation formula

replaces the integral in Equation (8) with a sum j

$$Y_i = \sum_j T_j S_{ij} \tag{9}$$

where Y_i is the value of Y(V) corresponding to channel or pulse height i, T_j is the total number of gamma-rays in the energy interval ΔE_j about the energy E_j, and S_{ij} is the intensity in channel i for a gamma-ray of the jth energy group. In applying Shannon's Sampling Theorem to the analysis of spectra obtained with NaI(Tℓ) crystals, sampling components are chosen so that the energy intervals between the energy groups are less than the half width at half maximum of the photopeak at that energy (Linden, 1959; Trombka and Schmadebeck, 1968).

A valid numerical transformation can now be obtained using techniques derived from the analysis of variance. The details of this derivation can be found in Trombka et al (1970). Using the least square principle, the method requires that

$$M = \sum_i \omega_i (Y_i - \sum_j T_j S_{ij})^2 \tag{10}$$

be a minimum, where the statistical weight corresponding to the measurement of Y_i in channel i, $\omega_i = 1/\sigma_i^2$ (where σ_i^2 is the variance in the measurement of the count in channel i). The variance σ_i^2 data processing must include all effects such as background subtraction. The other terms have been defined. The partial derivatives of M are taken with respect to T in order to determine the minimum. The solution in matrix form is given by

$$T = (\tilde{S}\omega S)^{-1} \tilde{S}\omega Y \tag{11}$$

where Y is a vector describing the pulse height spectrum, S is an m x n matrix describing the discrete set of detector response function, $\tilde{S}$ is the transposition of S, ω is a square diagonal matrix of the weighting functions, and T is a best estimate of the differential energy photon spectrum. A detailed description of the calculating method and computer program is found in Trombka and Schmadebeck (1968).

We are now able to transform from measurement space to photon space. A major problem exists because we have a mixture of discrete lines and continuum. This problem is further complicated in the determinations of the inverse matrix $(\tilde{S}\omega S)^{-1}$. One obtains oscillations in the solution due to interference between the components of the S matrix. These oscillations become most pronounced in the vicinity of discrete lines. Methods for damping out these oscillations have been developed. Our method essentially consists in trying to obtain a description of the continuous component using the transposition from pulse height to energy space (Equation 11), eliminating all possible discrete lines and points on either side of those lines where oscillation occur, and finding the best fit of a simple spectrum, generally a power law distribution, to the remaining points. Our analytic methods allows the use of other types of analytic and empirical background shapes. In fact if one wishes, a number of interations on the analysis can be performed using various background shapes in order to find the form most suitable for the particular situation. For purposes of illustration of the analytical method we will assume the background can be described by a power

law distribution. We thus assume that the continuum can be approximated by the function

$$T_c = AE^{-n} \tag{12}$$

where A is an amplitude constant, and n is the power to be determined by fitting those points which characterize the continuous distribution.

Once T_c is determined, the corresponding pulse height distribution can be obtained by using Equation (9). The pulse height spectrum of T_c is then subtracted from the measured spectrum, and the pulse height distribution of the discrete component obtained. This can then be converted to a photon spectrum. The geochemical information can then be deduced from this final photon distribution.

An example of the use of the analytical method may be a help in understanding its application. Using the methods of the first part of this paper the discrete line gamma-ray emission spectrum from the lunar surface for a given composition can be obtained. An average lunar surface composition for the major elements composition was assumed and is indicated in Table 6. The expected photon flux is also given. For the neutron capture lines, the flux to weight ratios used were 1.4 of the Apollo 11 values. Using Monte Carlo methods, a pulse height spectrum due to the discrete lines observed at the orbital altitude with NaI(Tℓ) detector was generated. The detector resolution for 0.661 MeV was a 2-3/4" by 2-3/4" assumed to be 8.5%. We now assumed that the continuum spectrum was of the form $T_c = AE^{-1.3}$. From the Luna 10 data (Vinogradov et al, 1967) we estimated

that the continuous distribution was about 85% of the total observed flux from the lunar surface. Finally, it was assumed that the spectrum was accumulated for 200 minutes. The calculated spectrum is the top curve shown in Figure 5. The spectrum was divided into 511 channels. Random fluctuations due to counting statistics were included. Instrument parameters correspond to the system used during the Apollo mission.

This pulse height spectrum was transformed back to a photon spectrum using a library of 118 monoenergetic components. The results are displayed in Figure 6. The oscillations around lines and at high energies can be easily seen. These oscillations and discrete lines were eliminated. Seventeen points remain to characterize the continuous distribution (the points circled). A least square fit was performed assuming a power law dependence. Both the magnitude A and power n were determined. For this example it was found that $A = 0.062$ and that $n = 1.33$, only 2.3% from the value assumed in the calculation. The calculated power law distribution of the continuum is shown as the line in Figure 6 and is assumed to extend up to 10 MeV. Using the values of A and n obtained from the least square fit, the shape and magnitude of the pulse height spectrum of the continuous spectrum can be obtained. It is the smooth middle curve of Figure 5. This component is subtracted from the top spectrum shown in Figure 5, and an estimate of the discrete line spectrum is obtained. This is the bottom curve of Figure 5.

To analyze this line spectrum, pulse height spectra characteristic of the elemental reaction components (rather than monoenergetic gamma-ray lines) are used for the library. All gamma-ray lines for natural radioactive decay, neutron capture, and neutron inelastic scatter for each element are grouped separately. For example the pulse height spectrum for the natural emission spectrum from Th and that expected from the O (n,xγ) reactions are shown in Figure 7. The set of components used to form a fifteen component library is shown in Table 6. Using this library, the elemental photon flux and elemental composition can be obtained by matrix inversion (Equation 11).

The results of the analysis of the discrete pulse height spectrum are given in Table 6. These recovered results can be compared with the values assumed in the calculation. If our assumptions about the continuum and discrete line spectra are correct, our capabilities for obtaining qualitative and quantitative elemental analysis from the measured gamma-ray are defined by these results and are discussed below.

The errors indicated in the table are associated with counting statistics, background subtraction, and mutual interference of components. Our ability to determine the natural radioactive elements, Th, U, and K should be limited only by counting statistics. The results agree well with the true values. The reactions Mg(n,nγ), Fe(n,nγ), and Si(n,nγ) can be used to determine the elemental weight fraction of Mg, Fe, and Si.

One of the major sources of error in the determination of the elemental weight fraction can be attributed to interference between various spectral shapes, that is the inability to resolve elemental components separately. An analysis of the co-variance between various elemental components making up the pulse height spectra of the libraries used in the analysis of the discrete spectra has been carried out and the percent interference between various components calculated. The method of calculation is described in Trombka and Schmadebeck (1968). The higher the percent interference, the more difficult is it to resolve the particular components. Our laboratory experience indicates that interferences greater than 20% cause trouble in interpretation. Table 7 indicates the percent interferences greater than 20% between the various library components used in the analysis of the elemental reaction pulse height spectra. For example one finds that the Fe(n,γ) spectrum strongly interferes with the O(n,xγ), and Si(n,nγ) and Al(n,γ) spectra. Thus it is hard to use these results to determine Fe concentration. This analysis also predicts difficulties in using other high energy lines. Some of the problem can be removed if it is possible to use plausible geochemical assumptions. For example, it might be reasonable to assign the concentration of Fe from the Fe(n,nγ) component, or of Si and O from general geochemical considerations.

Chi-square is also calculated to determine the goodness of fit. This parameter is of utmost interest in determining if there has been any significant change in the gain or zero level of the spectrometer, and whether a component or components are missing. For details on the application of these parameters see Trombka and Schmadebeck (1968) and Trombka et al (1970). Great care must be used in interpreting the Chi-square fit. A good fit does not necessary represent truth in terms of geochemical analysis. Thus using monoelemental library components in the least square fit, yield poorer Chi-square values than using monoenergetic library components but one obtains more physically meaningful results with the elemental library components.

The procedure described above illustrates one iteration on the data. In actual practice a number of iterations are used. For the second iteration one eliminates all monoelemental components with negative intensities or with intensities with an error greater than 100%. The remaining elemental components, which correspond for the most with the higher concentration elements, are then used to construct a composite discrete energy pulse height spectrum. This discrete pulse height spectrum is then subtracted from the original and a better estimate of the background continuum is obtained. The analysis as described above can then be repeated.

The procedure for analyzing the measured pulse height spectra described above allows us to perform analysis of the Apollo 15 and 16 gamma-ray spectra.

Both qualitative and quantitative results can be obtained. Accuracy and precision of results are determined in terms of counting statistics, background subtraction, and spectral interference.

DISCUSSION

Although we have discussed the use of "ground truth" above, we must return to it at this stage. The matrix inversion program can make some use of ground truth; for example, the ratio Th/U may be set at a geochemically known value around 3.8 or the concentration of O and Si may be assumed constant in starting an iteration. Beyond this, the final chemical concentrations derived may be compared with the soil analyses in suitable regions such as Mare Tranquillitatis. This has been and will be useful in developing the computer procedures to higher precision and accuracy. It may also be necessary at a future stage to introduce a scale factor for one or more elements whose analysis depends on cosmic-ray interaction, either because of deficiencies in the Reedy-Arnold model or limitations of our knowledge of cross-sections. Other sorts of experimental evidence may enter at this point. Simulation experiments using accelerators, and balloon flights which carry a detector-target package to the top of the earth's atmosphere are both important here.

While the general sky background seems to consist mainly of continuum, and hence is included in the empirically derived lunar continuum, its study is necessary as a check of our understanding. The spacecraft contributes a small

but measurable line spectrum. The lines of K and Th come from known sources and have been measured on the ground. Other lines are produced by cosmic-ray bombardment. All these are best extracted from the spectrum observed in transearth coast, since the continuum there is much lower in intensity than the lunar one. The corrections for K and Th are significant at the lowest levels observed on the moon.

At present the list of elements which can be determined with reasonable accuracy on the moon is as follows: Th, U, K, Si, O, Fe, Mg. As methods are refined the data already obtained are expected to yield more (Metzger, 1972).

For future missions, the use of a Ge(Li) detector system, possibly with collimation to improve areal resolution, would be a major improvement. The much higher energy resolution would greatly simplify the required data analysis.

In extending the process to other objects in the solar system, there are a few general guidelines. First, while the minimum necessary counting time for meaningful results on major elements will depend on closeness of approach, size of object, instrument design, and composition, the value observed so far in our Apollo analyses, of the order of 30 minutes, is encouraging for flyby missions to larger objects. The minimum time required for detailed mapping of an entire object on a resolution of the order of 5° will be of the order of a

month. Since the K/U ratio on the lunar surface is lower than that observed in meteorites or on earth, we might anticipate that the spectrum of another rocky object would show the K^{40} line at 1.46 MeV more prominently. The spectrum of an object much higher in hydrogen, such as a comet, will be qualitatively different, with neutron capture lines much more prominent. Finally, Mars is a special case, with an atmosphere comparable to the mean thickness of the lower-energy gamma-ray lines. The experiment is still quite feasible; the special aspects are discussed elsewhere (Metzger et al, 1970; Surkov et al, 1971)

ACKNOWLEDGMENTS

We deeply appreciate the assistance of A. E. Metzger (Jet Propulsion Laboratory), T. W. Armstrong (Oak Ridge National Laboratory), R. E. Lingenfelter (University of California, Los Angeles), V. J. Orphan and J. John (Gulf Radiation Technology), G. A. Osswald (University of Cincinnati), M. Bielefeld and M. Silbergeld (Computer Science Corporation), M. J. Berger and S. M. Seltzer (National Bureau of Standards), and R. L. Schmadebeck (Goddard Space Flight Center).

This research was supported by NASA Contract NAS 9-10670.

REFERENCES

Armstrong, T. W., Calculation of the lunar photon albedo from galactic and solar proton bombardment, J. Geophys. Res., 77, 524, 1972.

Bartholomew, G. A., A. Dovieka, K. M. Eastwood, S. Mondaro, L. V. Groshev, A. M. Demidov, V. I. Pelekhov, and L. L. Sokolovskii, Compendium of thermal-neutron-capture γ-ray measurements. Part I:$Z \leq 46$, Nuclear Data A3, 367, 1967.

Bell, P. R., Beta and Gamma-Ray Spectroscopy, pp. 132-164, edited by Kai Siegbahn, North Holland Publishing Co., Amsterdam, 1955.

Dickens, J. K., $^{28\text{-}30}$Si(n,xγ) reactions for $5.3 \leq E_n \leq 9.0$ MeV, Physical Review C, 2, 990, 1970.

Drake, M. K., Neutron and gamma-ray production cross-sections for sodium, magnesium, chlorine, potassium, and calcium; Vol. VI, Calcium, pp. 114, General Atomic Division of General Dynamics Corporation, Report GA-7829 (Nuclear Defense Laboratory Report NDL-TR-89, U. S. Army), 1967.

Drake, M. K., Neutron and gamma-ray production cross-sections for silicon, pp. 211, Gulf General Atomic Report GA-8628 (Defense Atomic Support Agency Report DASA 2099), 1968.

Finkel, R. C., J. R. Arnold, M. Imamura, R. C. Reedy, J. S. Fruchter, H. H. Loosli, J. C. Evans, A. C. Delany, and J. P. Shedlovsky, Depth variation of cosmogenic nuclides in a lunar surface rock and lunar soil, Proc. Second Lunar Sci. Conf., Geochim. Cosmochim. Acta Suppl. 2, Vol. 2, 1773, MIT Press, 1971.

Gorenstein, P. and P. Bjorkholm, Alpha-particle spectrometer experiment, Apollo 15 Preliminary Science Report, NASA Report SP-289,18-1, 1972.

Gorenstein, Paul, and Herbert Gursky, Characteristic γ- and x-radiation in the planetary system, Space Science Reviews, 10, 770, 1970.

Hubbard, N. J., and P. W. Gast, Chemical composition and origin of nonmare lunar basalts, Proc. Second Lunar Sci. Conf., Geochim. Cosmochim. Acta Suppl. 2, Vol. 2, 999, MIT Press, 1971.

Lederer, C. M., J. M. Hollander, and I. Perlman, Table of Isotopes, Sixth Edition, pp. 594, John Wiley & Sons, Inc., New York, 1967.

Linden, D. A., Discussion of sampling theorem, Proc. IRE, 47, 39, 1959.

Lingenfelter, R. E., E. H. Canfield, and V. E. Hampel, The lunar neutron flux revisited, Earth and Planetary Science Letters, 16, 355, 1972.

Lingenfelter, R. E., E. H. Canfield, and W. N. Hess, The lunar neutron flux, J. Geophys. Res., 66, 2665, 1961.

Maddison, R. J., and P. M. V. Jones, A measurement in GLEEP of the thermal neutron absorption cross-section of a sample of highly purified silicon, pp. 5, Atomic Energy Establishment, Winfrith, England, Report AEEW-M-887, 1969.

Mason, Brian, Meteorites, pp. 274, John Wiley and Sons, Inc., New York, 1962.

Metzger, A. E., "I feel like a banker," private communication, April 29, 1972.

Metzger, A. E., E. C. Anderson, M. A. Van Dilla, and J. R. Arnold, Detection of an interstellar flux of gamma-rays, Nature, 204, 766, 1964.

Metzger, A. E., and J. R. Arnold, Gamma-ray spectroscopic measurements of Mars, Applied Optics, 9, 1289, 1970.

Metzger, A. E., J. I. Trombka, L. E. Peterson, R. C. Reedy, and J. R. Arnold, Lunar Surface radioactivity: Preliminary results of the Apollo 15 and Apollo 16 gamma-ray spectrometer experiments, Science, 179, 800, 1973.

Orphan, V. J., and C. G. Hoot, Gamma-ray production cross-section for iron and aluminum, Gulf RT-A10743, pp. 199, 1971.

Orphan, V. J., C. G. Hoot, and J. John, Gamma-ray production cross-sections for the $^{16}O(n,x\gamma)$ reaction from 6.35-16.52 MeV neutron energy, Nucl. Sci. Eng., 42, 352, 1970.

Reedy, R. C., and J. R. Arnold, Interaction of solar and galactic-cosmic-ray particles with the moon, J. Geophys. Res., 77, 537, 1972.

Rossi, Bruno, High-Energy Particles, 569 pp., Prentice-Hall, Englewood Cliffs, N. J., 1952.

Schnetzler, C. C., and D. F. Nava, Chemical composition of Apollo 14 soils 14163 and 14259, Earth and Planetary Science Letters, 11, 345, 1971.

Seltzer, S. M., and M. J. Berger, Response of NaI detectors to high-energy gamma-rays, ANS Transactions, 14, No. 1, 124, 1971.

Stehn, J. R., M. D. Goldberg, B. A. Magurno, and R. Weiner-Chasman, Neutron cross-sections, Volume I, Z = 1 to 20, Brookhaven National Lab. Rept. BNL-325, 1964.

Surkov, Yu.A., L. P. Moskaleva, A. N. Khalemsky, and V. P. Kharyukova, On gamma-radiation of the atmosphere and surface of Mars, Space Research XI, Volume 1, 181, edited by K. Ka. Kondratyev, M. J. Rycroft, C. Sagan, Akademie-Verlag, Berlin, 1971.

Trombka, J. I., E. Eller, G. A. Osswald, M. J. Berger, and S. M. Seltzger, ^{252}Cf neutron induced radioactive capture gamma-rays for high energy detector calibration, USAEC Report CONF-710402, Vol. III, III-43, 1971.

Trombka, J. I., and R. L. Schmadebeck, A Numerical Least-Square Method for Resolving Complex Pulse Height Spectra, pp.170, NASA Report SP-3044, 1968.

Trombka, J. I., F. Senftle, and R. Schmadebeck, Neutron radioactive capture methods for surface elemental analysis, Nucl. Instr. and Meth., 87, 37, 1970.

Turkevich, A. L., E. J. Franzgrote, and J. H. Patterson, Chemical compositions of the lunar surface in Mare Tranquillatis, Science, 165, 277, 1969.

Vinogradov, A. P., Yu.A. Surkov, G. M. Chernov, F. F. Kirnozov, and G. B. Nazarkina, Lunar gamma-radiation and the composition of the lunar rocks according to the results of a Luna-10 experiment, Cosmic Research (English Transl.), 5, 741, 1967.

Wahlen, M., M. Honda, M. Imamura, J. S. Fruchter, R. C. Finkel, C. P. Kohl, J. R. Arnold, and R. C. Reedy, Cosmogenic nuclides in football-sized rocks, Proc. of the Third Lunar Sci. Conf., Geochimica Cosmochim. Acta Suppl. 3, Vol. 2, 1719, MIT Press, 1972.

Webber, William, R., The spectrum and charge composition of the primary cosmic-radiation, Handbuch der Physik, XLVI/2, Cosmic-Rays III, 181, Springer-Verlag, Berlin, 1967.

White, G. R., X-ray attenuation coefficients from 10 keV to 100 MeV, pp. 104, Natl. Bur. Standards (U.S.) Rept. 1003, 1952.

Wood, J. A., J. S. Dickey, Jr., U. B. Marvin, and B. N. Powell, Lunar anorthosites and a geophysical model of the moon, Proc. of the Apollo 11 Lunar Sci. Conf., Geochim. Cosmochim. Acta Suppl. 1, Vol. 1, 965, 1970.

Table 1

Gamma-ray fluxes from the decay of natural radioactivities. The half-lives used for K^{40}, Th^{232}, and U^{238} were 1.26×10^9, 1.41×10^{10}, and 4.51×10^9 years, respectively, and the K^{40}/K ratio used was 0.000118. The fluxes are for the Apollo 11 chemical composition (K, Th, and U values of 1150, 2.1, and 0.55 ppm by weight, respectively).

Parent Element	Isotope	Energy (MeV)	Yield/ disintegration	Flux (photons/ cm^2min.)
K	K^{40}	1.46	0.11	2.37
Th	Tl^{208}	2.614	0.36	2.41
	Ac^{228}	1.593	0.045	0.24
	Ac^{228}	0.97	0.20	0.82
	Ac^{228}	0.91	0.23	0.92
	Bi^{212}	0.727	0.07	0.25
	Tl^{208}	0.583	0.31	1.02
	Tl^{208}	0.511	0.083	0.26
	Ac^{228}	0.337	0.15	0.39
	Pb^{212}	0.239	0.47	1.06
U	Bi^{214}	2.204	0.05	0.24
	Bi^{214}	1.764	0.17	0.74
	Bi^{214}	1.378	0.05	0.19
	Bi^{214}	1.238	0.06	0.22

Table 1 (Continued)

Parent Element	Isotope	Energy (MeV)	Yield/ disintegration	Flux (photons/ $cm^2 min.$)
	Bi^{214}	1.12	0.17	0.59
	Bi^{214}	0.769	0.05	0.15
	Bi^{214}	0.609	0.47	1.24
	Pb^{214}	0.352	0.36	0.76
	Pb^{214}	0.295	0.19	0.37

Table 2

Chemical compositions used in calculations. Abundances of elements are in percent or parts per million (ppm) by weight.

	Apollo 11	Apollo 12	Apollo 14	Lunar Anorthosite	Chondrite
O	41.6	42.6	44.2	45.0	35.0
Na	0.32	0.32	0.47	0.3	0.68
Mg	4.6	6.3	5.6	2.4	14.4
Al	7.1	6.8	9.2	16.0	1.3
Si	20.0	21.4	22.5	20.7	18.0
K	0.115	0.18	0.43	~0.04	0.086
Ca	8.6	7.2	7.6	11.5	1.4
Ti	4.6	1.7	1.0	0.2	0.08
Fe	12.3	12.0	8.0	2.7	25.0
P(ppm)	600	1200	2100	400	1000
S(ppm)	1000	--	--	--	23000
Cr(ppm)	1950	2900	1300	--	2500
Mn(ppm)	1600	1700	1000	--	2600
Ni(ppm)	240	160	--	--	13000
Gd(ppm)	17	20	35	~1	0.34
Th(ppm)	2.1	8	14	~0.7	0.04
U(ppm)	0.55	2	4	~0.2	0.013
Sum	99.78	99.10	99.45	98.88	100.16

Table 3

Gamma-ray fluxes from solar-cosmic-ray produced radionuclides. The results are given for three different incident solar proton exponential rigidity spectral shapes and for 4π integral proton fluxes above 10 MeV of 100 protons/cm^2sec. The gamma-ray fluxes are for the Apollo 11 chemical composition.

Target	Radionuclide	Energy (MeV)	Fluxes (Photons/cm^2min)		
			R_0 = 50 MV	100 MV	150 MV
Na	Na^{22}	1.275	0.008	0.022	0.032
Mg	Na^{22}	1.275	0.024	0.102	0.189
Al	Na^{22}	1.275	0.016	0.084	0.152
	Al^{26}	1.809	0.149	0.360	0.518
Si	Na^{22}	1.275	0.012	0.104	0.241
	Al^{26}	1.809	0.078	0.378	0.689
Ti	V^{48}	0.983	0.183	0.175	0.162
	V^{48}	1.312	0.183	0.177	0.165
Fe	Mn^{54}	0.835	0.033	0.140	0.240
	Co^{56}	0.847	0.340	0.334	0.306
	Co^{56}	1.238	0.235	0.233	0.215

Table 4

Gamma-ray fluxes for lines resulting from galactic-cosmic-ray induced inelastic scattering and radioactivities. References are the sources for the cross-sections used in calculating the production rates for these reactions. The fluxes are for the Apollo 11 chemical composition and are in order of decreasing intensity for each element.

Reaction	Energy (MeV)	Flux (Photons/cm^2 min)
$O^{16}(n, n\gamma)^{(a)}$	6.129	2.43
$O^{16}(n, n\gamma)^{(a)}$	7.117	0.94
$O^{16}(n, n\gamma)^{(a)}$	6.917	0.79
$O^{16}(n, \alpha\gamma)^{(a)}$	3.68	0.56
$O^{16}(n, n\gamma)^{(a)}$	2.743	0.46
$O^{16}(n, n\alpha\gamma)^{(a)}$	4.433	0.44
$O^{16}(n, \alpha\gamma)^{(a)}$	3.85	0.28
$O^{16}(n, p)N^{16(b)}$	6.129	0.26
$O^{16}(n, \alpha\gamma)^{(a)}$	3.09	0.19
$Mg^{24}(n, n\gamma)^{(b)}$	1.369	0.78
$Mg^{24}(n, p)Na^{24(b)}$	2.754	0.12
$Al^{27}(n, n\gamma)^{(c)}$	2.21	0.43
$Al^{27}(n, n\gamma)^{(c)}$	1.013	0.40
$Al^{27}(n, n\gamma)^{(c)}$	3.001	0.28

Table 4 (Continued)

Reaction	Energy (MeV)	Flux (Photons/cm^{2}min)
$Al^{27}(n, 2n)Al^{26}$[d]	1.809	0.19
$Al^{27}(n, n\gamma)$[c]	0.843	0.16
$Al^{27}(n, \alpha)Na^{24}$[b]	2.754	0.13
$Si^{28}(n, n\gamma)$[e]	1.779	2.65
$Si^{28}(n, p)Al^{28}$[b]	1.779	0.72
$Si^{28}(n, p\alpha)Na^{24}$[f]	2.754	0.31
$Si^{28}(n, p2n)Al^{26}$[d]	1.809	0.31
$Si^{28}(n, n\gamma)$[e]	2.835	0.27
$Ca^{40}(n, n\gamma)$[g]	3.73	0.22
$Ca^{40}(n, n\gamma)$[g]	3.90	0.13
$Ti^{48}(n, n\gamma)$[f]	0.983	0.29
$Fe^{56}(n, n\gamma)$[c]	0.847	1.53
$Fe^{56}(n, n\gamma)$[c]	1.238	0.37
$Fe^{56}(n, n\gamma)$[c]	1.811	0.16
$Fe^{56}(n, n\gamma)$[c]	2.113	0.12
$Fe(n, x)Mn^{54}$[d]	0.835	0.11

[a]Orphan, Hoot, and John (1970)

[b]Stehn et al (1964)

[c]Orphan and Hoot (1971)

[d]Reedy and Arnold (1972)

Table 4 (Continued)

[e]Dickens (1970) for neutron energies below 10 MeV and Drake (1968) for neutron energies from 10 to 20 MeV

[f]Cross-sections estimated from analogous reactions

[g]Drake (1967)

Table 5

Gamma-ray fluxes for lines resulting from neutron capture. The results are for the Apollo 11 chemical composition. See the text for discussion about neutron capture in other chemical compositions.

Source	Energy (MeV)	Yield/Capture	Flux (photons/cm^2min)
Mg(n,γ)	3.92	0.36	0.02
Al(n,γ)	7.724	0.23	0.09
Al^{28}	1.779	1.00	0.14
Si(n,γ)	4.936	0.53	0.34
	3.54	0.53	0.27
Ca(n,γ)	6.42	0.40	0.22
	1.943	0.89	0.21
Ti(n,γ)	6.755	0.47	1.67
	6.42	0.31	1.07
	1.38	0.86	0.97
Fe(n,γ)	9.298	0.03	0.12
	7.643	0.21	0.75
	7.629	0.21	0.75
	7.277	0.05	0.18
	6.018	0.08	0.25
	5.92	0.08	0.25

Table 6

Synthetic and Recovered Weight Fractions and

Fluxes for An Average Lunar Composition

Element	Synthetic		Recovered
	Flux, (photons/cm^2 min)	Weight Fraction	Weight Fraction
Th	8.44	2.1(ppm)	2.11 ± 0.14
U	5.21	0.55(ppm)	0.53 ± 0.04
K-40	2.37	1150(ppm)	1168 ± 92
O(n,xγ)	6.60	0.42	0.49 ± 0.05
Mg(n, nγ)	1.32	0.05	0.060 ± 0.012
Al(n, nγ)	3.06	0.10	0.15 ± 0.02
Al(n, γ)	0.70	0.10	0.15 ± 0.17
Fe(n, nγ)	2.23	0.10	0.10 ± 0.01
Fe(n, γ)	3.10	0.10	0.14 ± 0.02
Si(n, nγ)	5.49	0.21	0.21 ± 0.03
Si(n, γ)	1.27	0.21	0.35 ± 0.08
Ca(n, nγ)	0.48	0.09	0.22 ± 0.07
Ca(n, γ)	0.84	0.09	0.11 ± 0.05
Ti(n, nγ)	0.16	0.015	0.010 ± 0.003
Ti(n, γ)	1.88	0.015	0.011 ± 0.005

Table 7

Percent Interference Between Library Components

	Th	Mg (n, nγ)	U	O (n,xγ)	Al (n, nγ)	Fe (n, nγ)	Si (n, nγ)	Ca (n, nγ)	Ti (n, nγ)	Al (n, γ)	Si (n, γ)	Ca (n, γ)	Ti (n, γ)	Fe (n, γ)	K^{40}
Th	100		20.2												
Mg(n, nγ)		100		21.0					29.9						
U	20.2		100												
O(n,xγ)		21.0		100				31.5					51.2	22.4	
Al(n, nγ)					100										
Fe(n, nγ)						100									
Si(n, nγ)							100			73.6				56.7	
Ca(n, nγ)				31.5				100						21.5	
Ti(n, nγ)									100						
Al(n, γ)							73.6			100				79.2	
Si(n, γ)											100				
Ca(n, γ)												100			
Ti(n, γ)		29.9		51.2									100		
Fe(n, γ)				22.4			56.7	21.5		79.2				100	
K^{40}															100

FIGURE CAPTIONS

Figure 1. The calculated gamma-ray fluxes for the indicated chemical compositions at an isotropic detector just above the moon's surface (2π geometry). Except for the line at 0.511 MeV, the fluxes are for the discrete lines produced by the decay of naturally occurring radionuclides (Table 1) and from the interaction of GCR and SCR particles with the moon (Tables 3-5). The data are grouped in energy intervals 50 keV wide. Note that the flux scale is the same as that in Fig. 2.

Figure 2. The calculated gamma-ray fluxes for the indicated chemical compositions at an isotropic detector just above the moon's surface (2π geometry). Except for the line at 0.511 MeV, the fluxes are for the discrete lines produced by the decay of naturally occurring radionuclides (Table 1) and from the interaction of GCR and SCR particles with the moon (Tables 3-5). The data are grouped in energy intervals 50 keV wide. Note that the flux scale is the same as that in Fig. 1.

Figure 3. The top diagram shows the angles (β and θ) and distances for a detector at an altitude h above the moon relative to a point source on its surface. The graph shows the relative fluxes at an isotropic detector from a point source (I', Equation 6), from inside a circle,

and from beyond a great circle boundary, as a function of the distance along the surface of the moon from the sub-detector point. The fluxes are for an altitude of 100 km above the moon (R_{moon} = 1738 km) and for four different profiles for gamma-ray source intensity versus depth.

Figure 4. The pulse height spectra for monoenergetic gamma-rays at 3 different energies incident upon a 3 by 3 inch NaI(Tℓ) detector (~19 keV/channel). The important spectral features are identified. These spectra are theoretical Monte Carlo calculations.

Figure 5. The top curve is a pulse height spectrum calculated for the average lunar chemical composition given in Table 6 and includes both discrete lines and continuum as described in the text. This spectrum is for a 2-3/4 by 2-3/4 inch NaI(Tℓ) crystal (~19 keV/channel) and includes statistical errors appropriate for a 200 min. integration time. The middle curve is the pulse height spectrum of the continuum shown in Fig. 6. The bottom curve is the pulse height spectrum for the discrete lines obtained when the continuum contribution is subtracted from the original spectrum (top curve).

Figure 6. The dots are the lunar photon spectrum obtained when the synthesized lunar pulse height spectrum (top curve, Fig. 5) was transformed

by a matrix inversion (Equation 11) using 118 monoenergetic components. The 17 circles are the intensities at energies where there are no discrete lines used to obtain the continuum and the straight line is the least squares fit to these points, the best fit being $T_c = 0.062\ E^{-1.33}$.

Figure 7. The pulse height spectra used for the monoelemental components Th and O(n,xγ), calculated for a 2-3/4 by 2-3/4 inch NaI(Tℓ) detector (~19 keV/channel). These components, along with those for the other elemental components given in Table 6, were used for the matrix inversion of the discrete pulse height spectrum (bottom curve, Fig. 5) in obtaining the results given in Table 6.

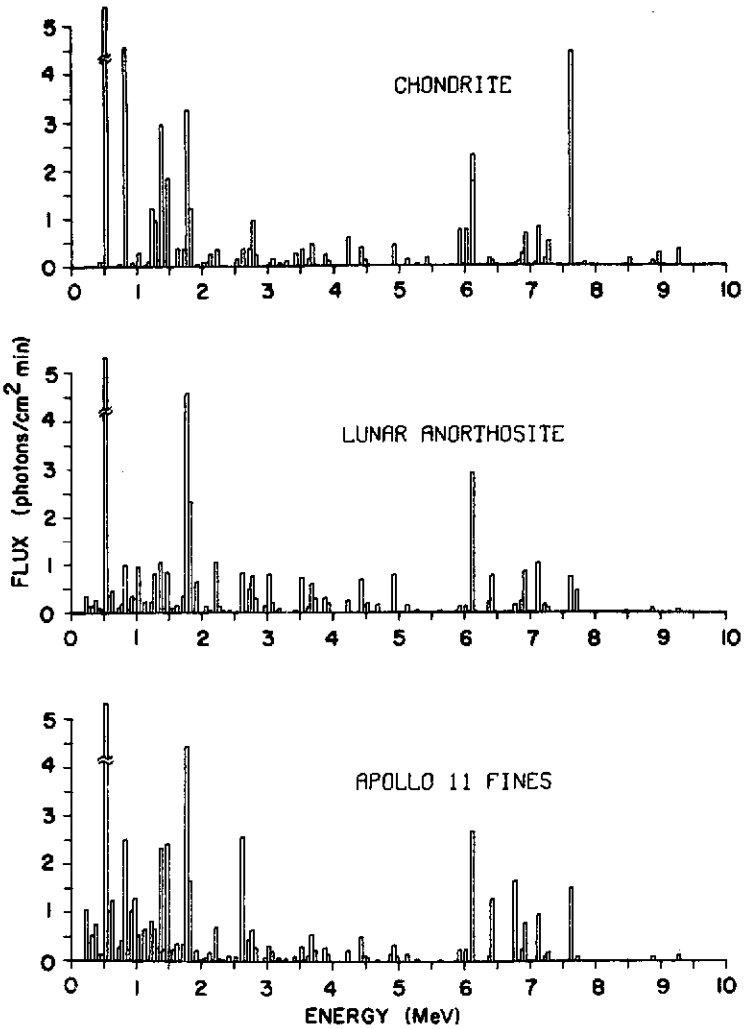
CHONDRITE
LUNAR ANORTHOSITE
APOLLO 11 FINES
FLUX (photons/cm² min)
ENERGY (MeV)
0
1
2
3
4
5
6
7
8
9
10

Figure 1

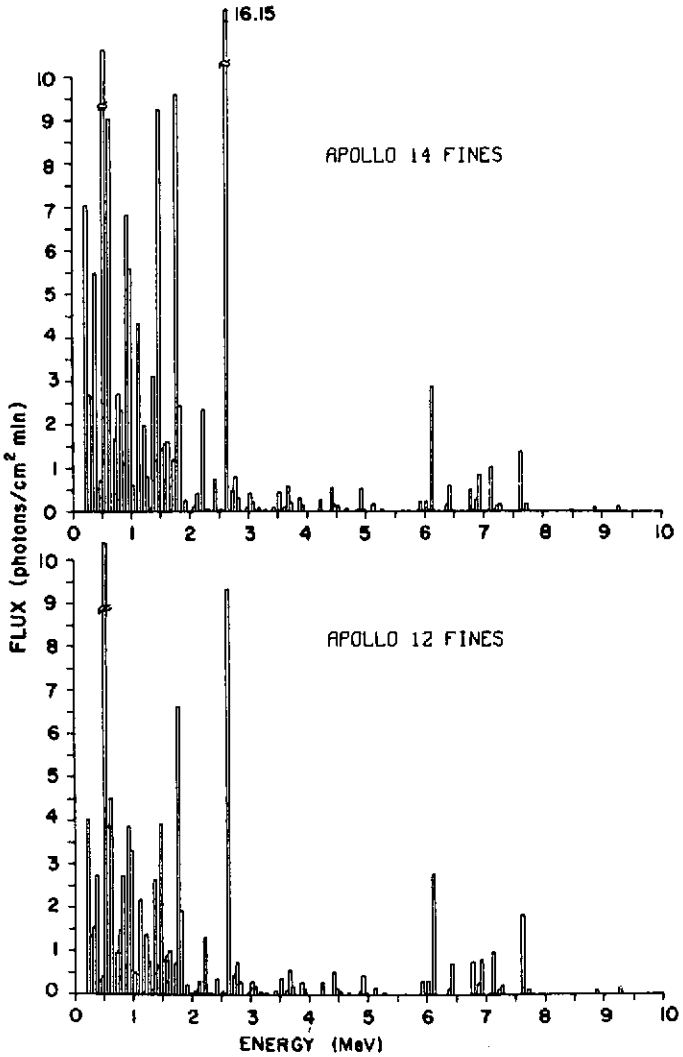
16.15
APOLLO 14 FINES
APOLLO 12 FINES
FLUX (photons/cm² min)
ENERGY (MeV)

Figure 2

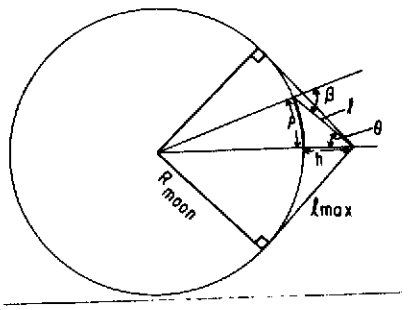
β
l
ρ
θ
h
R moon
ℓmax

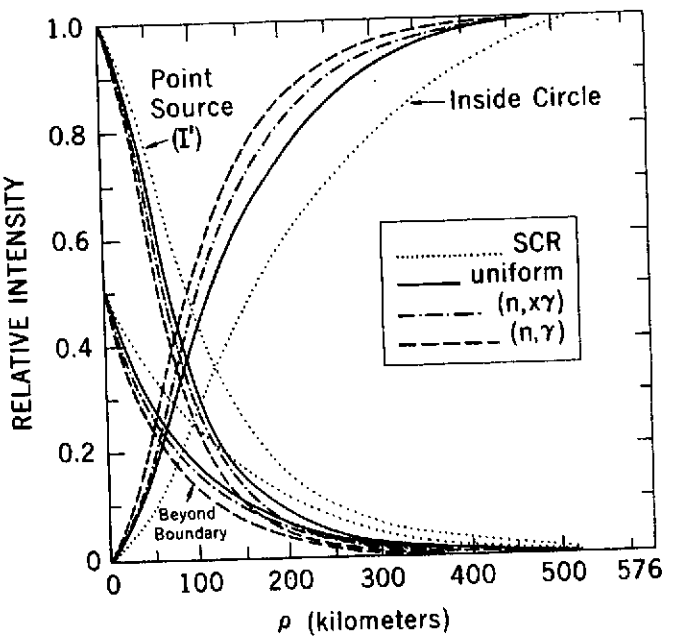
1.0
0.8
0.6
0.4
0.2
0
RELATIVE INTENSITY
Point
Source
(I')
Inside Circle
SCR
uniform
(n,xγ)
(n,γ)
Beyond
Boundary
0
100
200
300
400
500
576
ρ (kilometers)

Figure 3

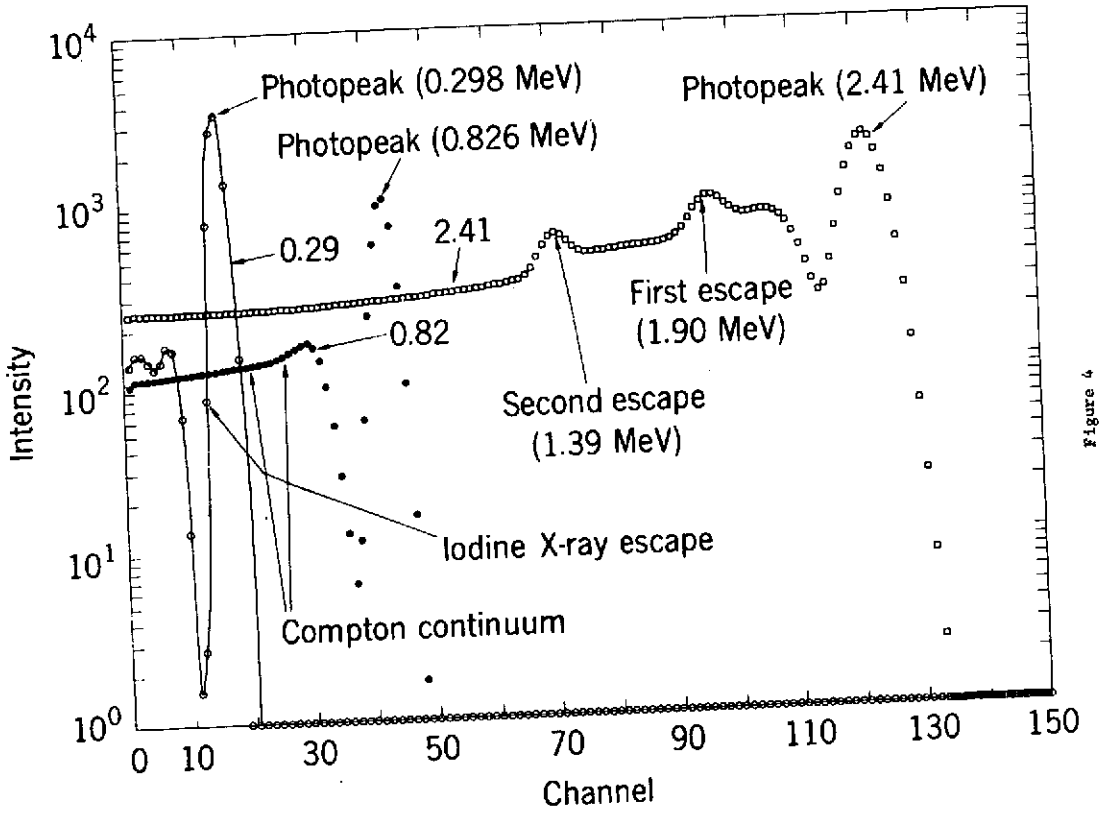
Photopeak (0.298 MeV)
Photopeak (0.826 MeV)
Photopeak (2.41 MeV)
0.29
2.41
0.82
First escape
(1.90 MeV)
Second escape
(1.39 MeV)
Iodine X-ray escape
Compton continuum
Intensity
Channel
10^4
10^3
10^2
10^1
10^0
0
10
30
50
70
90
110
130
150

Figure 4

62

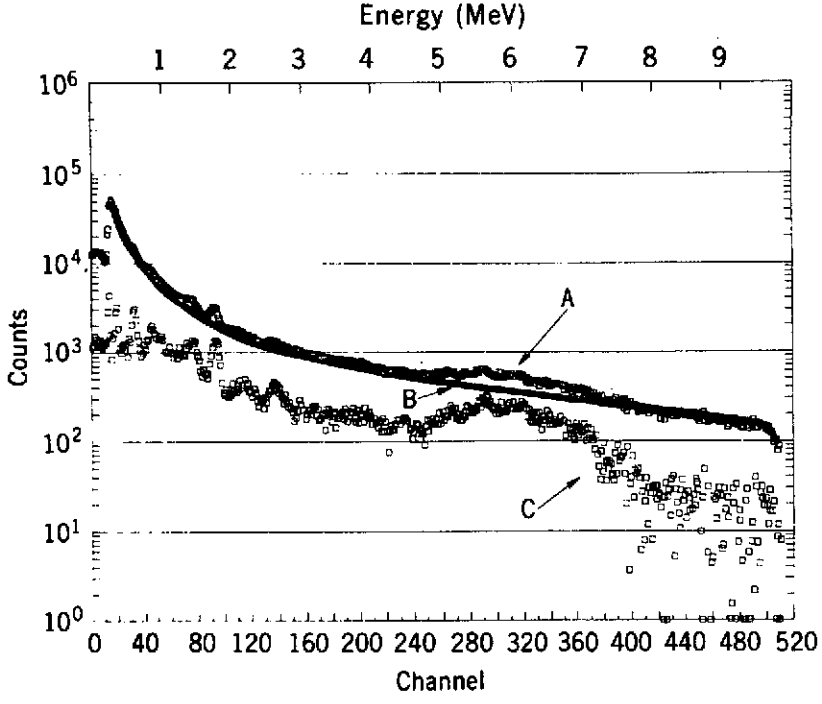

A is the total lunar emission pulse height spectrum
B is the pulse height spectrum of continuum lunar background
C is the pulse height spectrum of the discrete line lunar emission

Figure 5

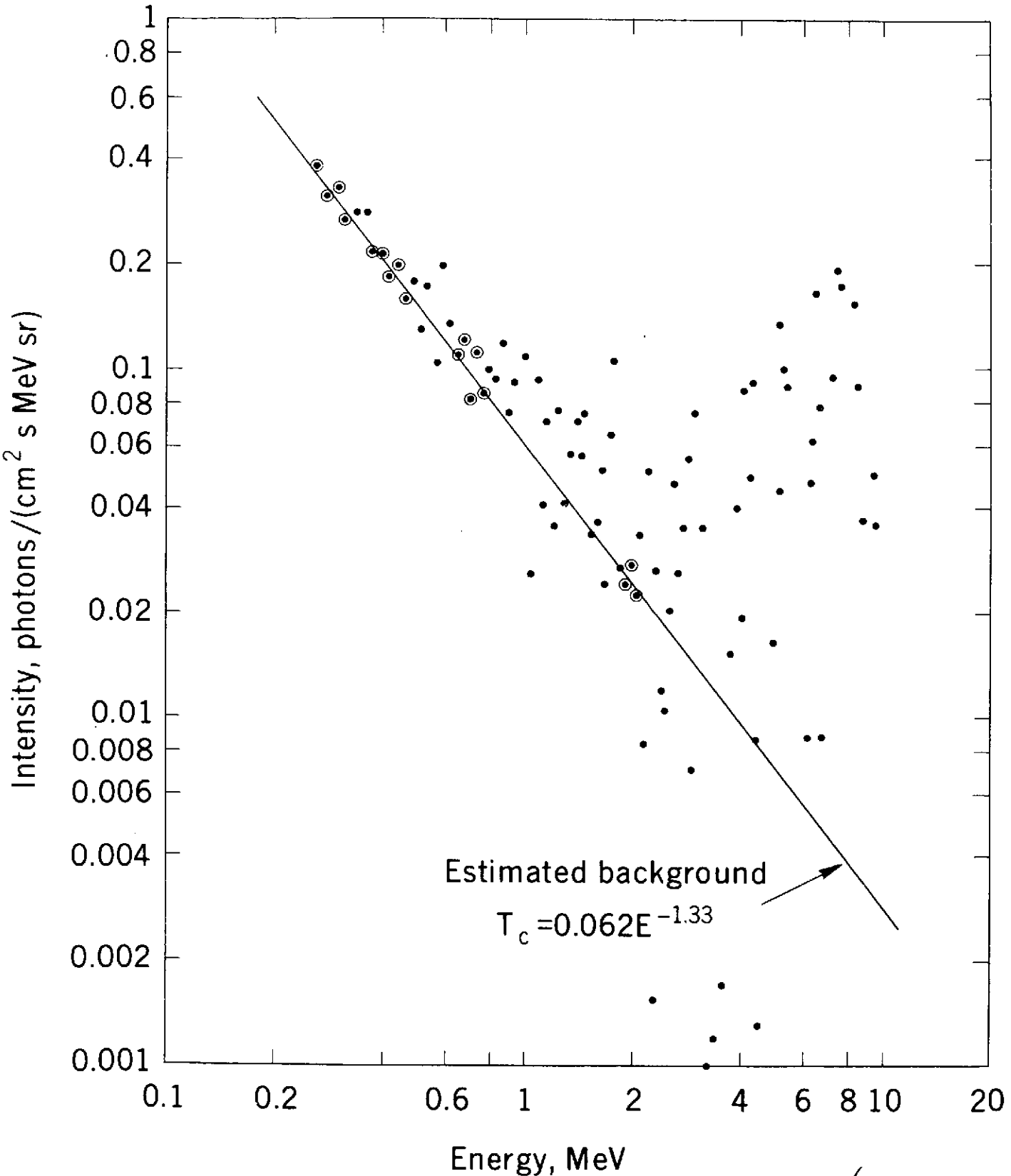
Intensity, photons/(cm^2 s MeV sr)
1
0.8
0.6
0.4
0.2
0.1
0.08
0.06
0.04
0.02
0.01
0.008
0.006
0.004
0.002
0.001
0.1
0.2
0.6
1
2
4
6
8
10
20
Energy, MeV
Estimated background
$T_c = 0.062E^{-1.33}$

64

FIGURE 6

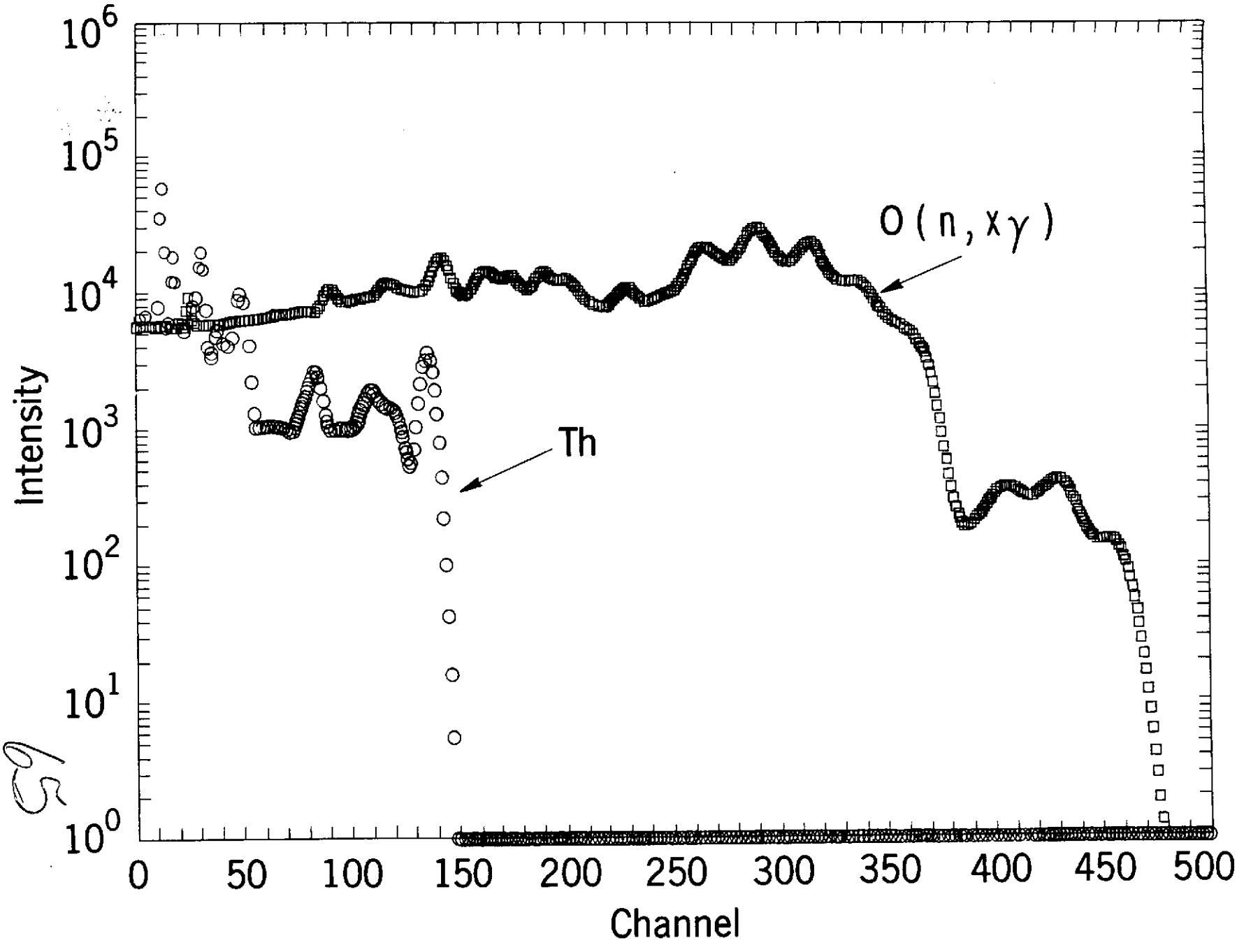
10^6
10^5
10^4
10^3
10^2
10^1
10^0
Intensity
O(n, xγ)
Th
0
50
100
150
200
250
300
350
400
450
500
Channel

FIGURE 7